Supplementary Material: Isotope study of the nonlinear pressure shifts of ^{85}Rb and ^{87}Rb hyperfine resonances in Ar, Kr, and Xe buffer gases

B. H. McGuyer[a)]
Department of Physics, Princeton University, Princeton, New Jersey 08544, USA
(*Electronic mail: bmcguyer@amazon.com.)

(Dated: 25 March 2023)

CONTENTS

S-I. AVERAGING OVER THE DIRECTION OF ROTATION

The rotational wave function $|\psi_N\rangle$ may be decomposed in terms of orthonormal Hund's case (b) rotational spin basis functions $|Nn\rangle$ with $\Lambda = 0$ as $|\psi_N\rangle = \sum_n B_n |Nn\rangle$, with $n = m_N$.[1] Each sticking collision then corresponds to a choice of coefficients B_n. To average over the direction of rotation, we need to determine the statistical weights $\langle B_n B_m^* \rangle$ to use with (11).

To proceed, consider using an operator $\mathbf{R}(\theta,\phi,\psi)$ with Euler angles (θ,ϕ,ψ) to rotate an arbitrary $|\psi_N\rangle$ to a new direction. After this rotation, the coefficients are $B_n(\theta,\phi,\psi) = \sum_m B_m(0,0,0) D^{(N)}_{n,m}(\theta,\phi,\psi)$, where the Wigner "big" D-function $D^{(N)}_{n,m}(\theta,\phi,\psi) = \langle Nn|\mathbf{R}(\theta,\phi,\psi)|Nm\rangle$. Averaging uniformly over all Euler-angle values then gives $\langle B_n B_m^* \rangle = \delta_{n,m}/[N]$ from D-function orthogonality.

Therefore, the substitution (33) averages over the direction of rotation.

S-II. ESTIMATES FOR THE DIPOLAR- AND QUADRUPOLAR-HYPERFINE INTERACTIONS

Ref. 2 provides estimates for the strength of the dipolar- and quadrupolar-hyperfine interactions for ^{85}Rb with ^{131}Xe. We can use this to estimate parameter values as follows:

For the dipolar interaction, noting that the coefficient $t_0(R) = B_a(R)$ in Eq. (31) of Ref. 2, Fig. 14 of Ref. 2 estimates $|t_0(R)| \leq |\gamma(R)|$ for $R \in [2, 4.5]$ Å, which is just before the potential well in $V(R)$.[3] Approximating equality across R, this gives a rough estimate of $|(\psi p)_{\rm dh}| \leq |(\psi p)_{\rm sr}|/(\langle N\rangle g_I) \approx 0.5$ rad Torr for Rb in Xe using values in Table II. The values in Table V are reasonably comparable to this rough estimate.

For the quadrupolar interaction, noting that the coefficient $C_a(R) = eq_0(R)Q/\{4I(2I-1)\}$ in Eq. (31) of Ref. 2, Fig. 14 of Ref. 2 estimates $|C_a(R)| \leq |\gamma(R)/20|$ for $R \in [2, 3.5]$ Å, which again is just before the potential well in $V(R)$.[3] Approximating equality across R, this gives a rough estimate of $|(\psi p)_{\rm qh}| \leq |(\psi p)_{\rm sr}| 4I(2I-1)/(20\langle N\rangle Q) \approx 0.5$ rad Torr/Barn for Rb in Xe using values in Table II. Attempts to fit the nonlinear shapes of both isotopes of Rb in Xe seemed to require values about 1000 times larger than this rough estimate.

S-III. PRESSURE-GAUGE LINEARIZATION CORRECTIONS

Fig. S1 shows the size of the corrections used to linearize the pressure gauges of both vapor cells.

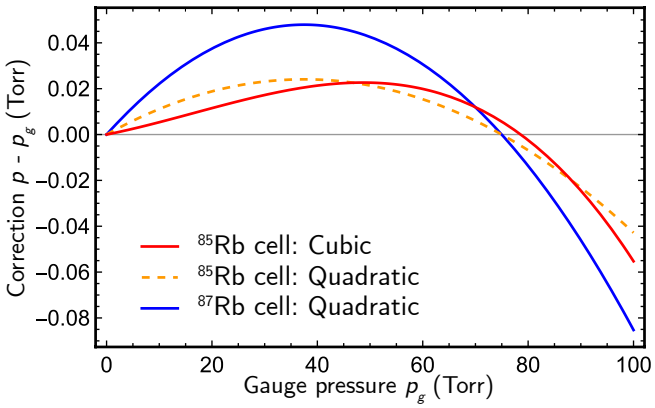

FIG. S1. Pressure-gauge linearization: The three curves show the size of the correction from the empirical formula (77) across the full manometer ranges for the three sets of coefficients in Table IV.

[a)]Present address: Amazon.com, Inc., 410 Terry Ave. North, Seattle, WA 98109.

S-IV. POSITIONAL SHIFT IN CAMPARO

Fig. S2 shows the proposed positional shifts in the Xe data from the analysis of Ref. 4 discussed in Section V.

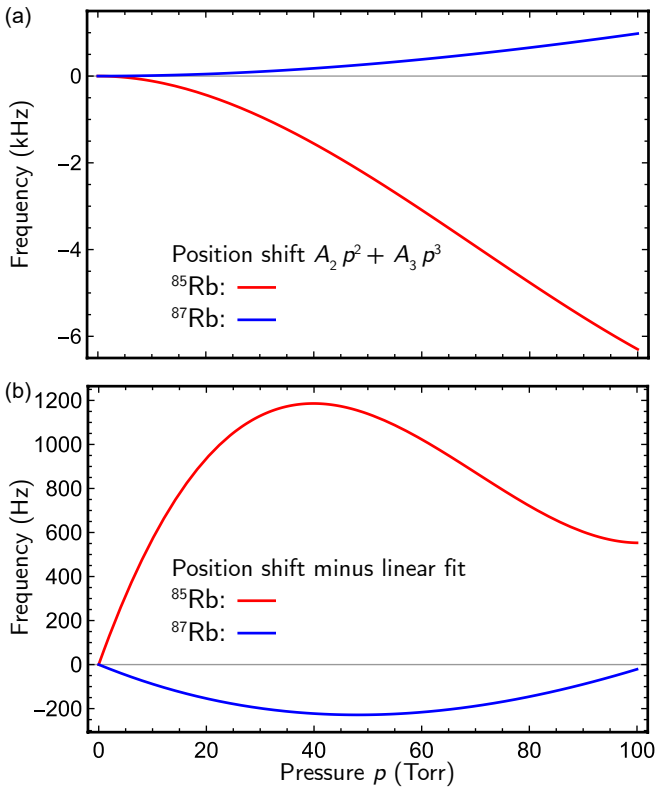

FIG. S2. Positional shifts in Ref. 4: (a) The curves show the positional shifts proposed for the Xe data. The form for the curves and the reported values for its A_2 and A_3 coefficients come from Eq. (68) and Table II in Ref. 4. (b) Example nonlinearity of the proposed positional shifts inferred by linear fitting, with the zero-pressure intercepts set to zero.

S-V. PREDICTIONS FOR VARIATION WITH TRANSITION AND APPLIED FIELD

Fig. S3 shows the predicted variation of the nonlinear shift with choice of α–β transition and applied field B. While only one Rb isotope is shown for each gas, the results are similar for the other isotopes. The curves come from (68) using the parameters in Table S1, so that their shapes for the 0–0 transition at zero field match those shown in previous plots. The results provide support for fitting the 0–0 transition data at $B = 1$ G with the negligible-field approximation (70). At zero field, the variation seems most apparent when comparing end resonances with the 0–0 transition, in particular, for ^{85}Rb in Xe. (^{87}Rb in Xe shows a similar but less striking variation because of its larger zero-field nonlinearity.) Likewise, the variation with applied field seems largest for end resonances, with a general trend of increasing the nonlinearity, though it may decrease it initially. This variation does

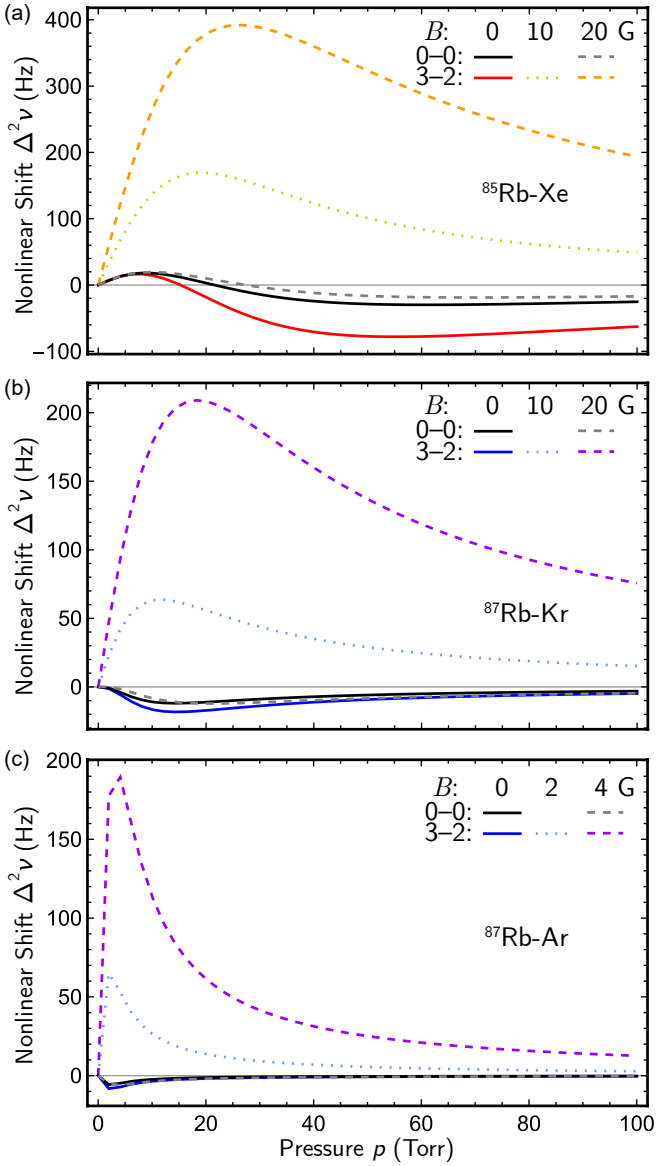

FIG. S3. Examples variations predicted for the nonlinearity with transition and applied field B: (a) Xenon. (b) Krypton. (c) Argon. The results for the Rb isotopes not shown were similar. At zero field, the nonlinearities varied the most between 0–0 and end resonances. End resonances show strong variation with applied field. Changing the sign of α and β or B often reflects the nonlinearity across the x-axis for large fields.

depend on the choice of transition (and field sign), with opposing end resonances appearing roughly as mirror images across $y = 0$ at large fields, as expected from the property $s_m(B) - s_m(0) \propto (\alpha + \beta)B$ from (69). Of the gasses, Ar seemed most sensitive to the field, likely because the quantity $[s_m(B) - s_m(0)]/[(\alpha + \beta)B]$ is roughly about 9 Hz/(Torr G) for Ar, compared to roughly 0.3 Hz/(Torr G) for the other gases.

S-VI. FIT PARAMETERS FOR PLOTTED CURVES

Table S1 provides parameters for the fitted shifts shown in Figs. 1, 5, 6, and S3, which differ slightly from the values reported in Table V that resulted from analyzing multiple data sets.

S-VII. FIT PARAMETERS FROM PREVIOUS WORK

For reference, Table S2 summarizes the results of Refs. 5 and 6, which analyzed the ^{85}Rb and ^{87}Rb data separately. Together, they provide an additional empirical summary of the data. For convenience, Figs. S4 and S5 reproduce two corresponding figures in Ref. 6. The parameters poorly describe the nonlinearity for ^{85}Rb in Xe, but do summarize the others well.

[1] J. M. Brown and A. Carrington, *Rotational Spectroscopy of Diatomic Molecules* (Cambridge University Press, Cambridge, 2003) Note that the definitions of **F** and **G** in this reference are swapped compared to their use in this work.

[2] T. G. Walker and W. Happer, "Spin-exchange optical pumping of noble-gas nuclei," Reviews of Modern Physics **69**, 629–642 (1997).

[3] A. A. Medvedev, V. V. Meshkov, A. V. Stolyarov, and M. C. Heaven, "Ab initio interatomic potentials and transport properties of alkali metal (M = Rb and Cs)–rare gas (Rg = He, Ne, Ar, Kr, and Xe) media," Physical Chemistry Chemical Physics **20**, 25974–25982 (2018).

[4] J. Camparo, "Nonlinear collision shifts of the 0–0 hyperfine transition due to van der Waals molecule formation," Journal of Chemical Physics **156**, 044303 (2022).

[5] B. H. McGuyer, T. Xia, Y.-Y. Jau, and W. Happer, "Hyperfine frequencies of ^{87}Rb and ^{133}Cs atoms in Xe gas," Physical Review A **84**, 030501(R) (2011).

[6] B. H. McGuyer, *Atomic physics with vapor-cell clocks*, Ph.D. thesis, Princeton University (2012).

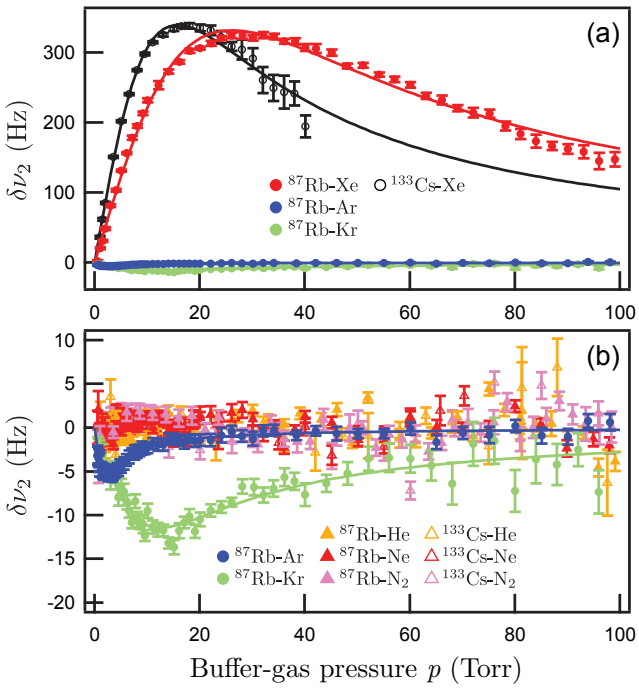

FIG. S4. Copy of Figure 4.6 in Ref. 6 (reproduced with permission): Summary of the nonlinear shifts $\delta\nu_2 = \nu - \nu_0 - sp$ for ^{87}Rb at 40.0° C and B = 1 G and for ^{133}Cs at 35.0° C and B = 0.2 G as reported in Ref. 6. (a) ^{87}Rb and ^{133}Cs in Xe, with ^{87}Rb in Ar and Kr for comparison. (b) ^{87}Rb in Ar and Kr, and ^{87}Rb and ^{133}Cs in He, Ne, and N_2. The solid curves are the fitting results reported in Ref. 6, which Table S2 summarizes for ^{87}Rb.

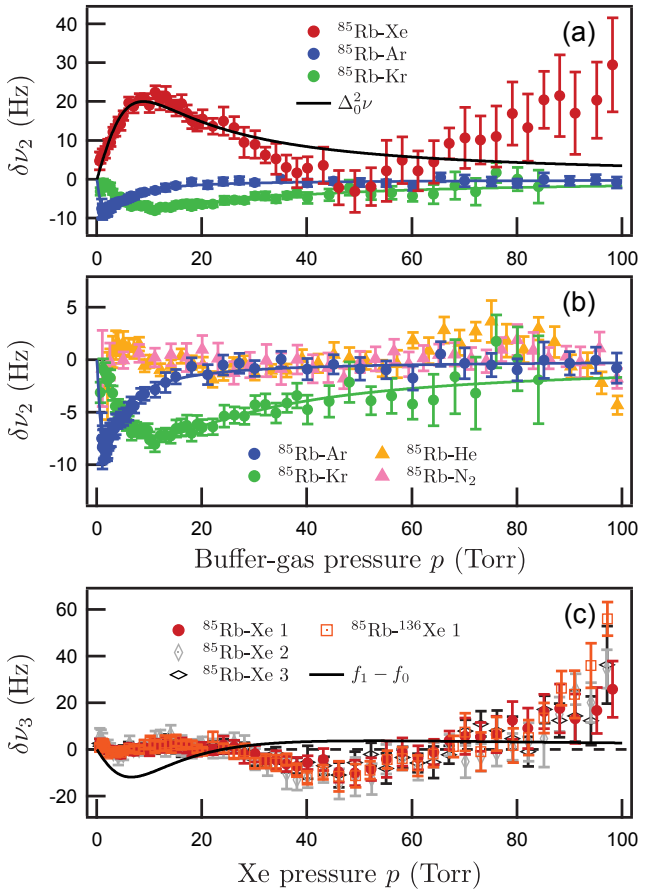

FIG. S5. Copy of Figure 4.7 in Ref. 6 (reproduced with permission): Summary of the nonlinear shifts $\delta\nu_2 = \nu - \nu_0 - sp$ for ^{85}Rb at 40.0° C and B = 1 G as reported in Ref. 6. (a) ^{85}Rb in Xe, with ^{85}Rb in Ar and Kr for comparison. (b) ^{85}Rb in Ar, Kr, He, and N_2. The solid curves in (a) and (b) are the fitting results reported in Ref. 6, which Table S2 summarizes. (c) The fit residuals $\delta\nu_3 = \delta\nu_2 - \Delta_0^2\nu$ for ^{85}Rb in Xe and ^{136}Xe, for fitting without the spin-rotation interaction. The solid curve is the difference of best-fit theoretical curves, with and without the spin-rotation interaction, which Table S2 summarizes. Three separate data sets demonstrate the repeatability of the measurements in natural abundance Xe. The residuals are unchanged with isotopically enriched ^{136}Xe.

TABLE S1. Fit parameters for the fitted curves shown in Figs. 1, 5, and 6. The values in Table V came from analyzing multiple data sets, so differ slightly from those given here.

Gas	$\sigma_b \times 10^9$ (Torr^{-1})	$\langle Tp^2 \rangle$ (ms Torr^2)	$(\psi p)_{\rm hfs}$ (ps Torr^{-1})	$(\psi p)_{\rm sr}$ (rad Torr)	$(\psi p)_{\rm dh}$ (rad Torr)	$(\psi p)_{\rm qh}$ (rad Torr Barn^{-1})	$\langle N \rangle$
Ar	-7.533	2.076	-0.672	-1.016	-0.626	0	∞
Kr	-81.598	64.916	11.282	9.61	-3.064	0	9.125
Xe	-169.115	54.333	-293.872	-31.9	-10.470	0	8.120

TABLE S2. Summary of fit parameters from previous works that separately analyzed the ^{85}Rb and ^{85}Rb data.[5,6] The hyperfine-shift and spin-rotation parameters were converted to the isotope-independent parameters of this work. Uncertainties for s were typically $\pm 0.25\%$.

Gas	Metal	s (Hz Torr^{-1})	$\langle Tp^2 \rangle$ (ms Torr^2)	$(\psi p)_{\rm hfs}$ (ps Torr^{-1})	$(\psi p)_{\rm sr}$ (rad Torr)	$(\psi p)_{\rm dh}$ (rad Torr)	$(\psi p)_{\rm qh}$ (rad Torr Barn^{-1})	$\langle N \rangle$
He	^{85}Rb	316.8	0	0	0	0	0	∞
He	^{87}Rb	714.2	0	0	0	0	0	∞
Ne	^{87}Rb	387.3	0	0	0	0	0	∞
N_2	^{85}Rb	229.6	0	0	0	0	0	∞
N_2	^{87}Rb	518.0	0	0	0	0	0	∞
Ar	^{85}Rb	-23.85	27.1 ± 4.5	88.1 ± 7.3	0	0	0	∞
Ar	^{87}Rb	-53.71	70 ± 12	51.5 ± 3.7	0	0	0	∞
Kr	^{85}Rb	-249.7	1500 ± 450	610 ± 100	0	0	0	∞
Kr	^{87}Rb	-558.1	1080 ± 310	291 ± 44	0	0	0	∞
Xe	^{85}Rb	-517.7	310 ± 75	-461 ± 58	0	0	0	∞
Xe	^{87}Rb	-1183.7	164 ± 13	-610 ± 28	0	0	0	∞
Xe	^{85}Rb	-517.9	2.2	-0.94	-31.9	0	0	∞
Xe	^{87}Rb	-1184.0	82 ± 10	-345 ± 35	-31.9	0	0	∞